Effect of Forward Speed on Roll Damping of a Container Ship Using URANS Simulations

Mohsin A. R. Irkal, S. Nallayarasu and S. K. Bhattacharyya

Abstract Ships are prone to large roll motions in beam and oblique seas at encounter frequencies near the design frequency of the vessel. The nonlinearity of roll damping and roll motion has been investigated in the past by various researchers. The prediction of roll damping and roll motion of ships becomes difficult by simplified approaches. Ship roll motion is highly influenced by viscous flow around the hull. Vortex formation and its shedding from the hull and appendages have larger contribution to roll damping. Therefore, the popular approach for prediction of roll damping and roll motion of ships is with the help of model experiments and more recently URANS (Unsteady Reynolds-averaged Navier–Stokes)-based simulations. Free roll decay experiments in calm water conditions give a good estimate of roll damping of ships at natural frequency. The flow characteristics around the hull may not be the same when the ship is moving at a forward speed. Hence, it is important to take into consideration the effect of forward speed on roll damping obtained from free roll decay of the ships. This paper addresses the effect of forward speed on roll damping of a 1:100 (Froude) scaled container ship model. The model is 2.88 m in length, 0.345 m in beam and was loaded to a draft of 0.12 m; free roll decay experiments at zero forward speed were carried out in a wave flume at Department of Ocean Engineering, IIT Madras. The wave flume is 4 m wide, 90 m long and has water depth of 2.5 m. The held-over free roll decay tests were carried out by subjecting the model to known initial heel and releasing it. The roll angle was measured using inclinometer via data acquisition CPU. The URANS-based simulations of the free roll decay experiments at zero forward speed were carried out in a commercial computational fluid dynamics (CFD) software and validated. The CFD model was then used to carry out the free roll decay simulations at two forward speeds of the ship model. The effect of forward speed on roll damping of the ship model was assessed from the results of CFD simulations.

Keywords Roll damping · Free roll decay · Container ship · Forward speed · CFD

M. A. R. Irkal (✉) · S. Nallayarasu · S. K. Bhattacharyya
Department of Ocean Engineering, Indian Institute of Technology Madras, Chennai 600036, India
e-mail: irkal.mohsin@gmail.com

K. Murali et al. (eds.), *Proceedings of the Fourth International Conference in Ocean Engineering (ICOE2018)*, Lecture Notes in Civil Engineering 22,
https://doi.org/10.1007/978-981-13-3119-0_12

1 Introduction

A seagoing vessel is expected to have lower amplitude motions for smooth operation of shipboard tasks, better crew efficiency and passenger comfort. A stable vessel also improves the fuel efficiency. It is desirable to understand the modes of motion of a floating body and predict its stability at the design stage. The seagoing vessels are prone to many environmental and man-made catastrophes. Extreme weather can cause fatal wave and wind loads on a floating body causing it to collapse. Roll motion is one of the major causes of accidents in slender floating bodies like ships. The other modes of motion of a ship except roll motion have better stability. This is because roll motion in ships suffers from both insufficient damping and restoring forces and moments. Especially, for the wave loads near roll resonance the roll acceleration of ships becomes highly undesirable and unsafe. The subject of roll motion and roll damping of ships has been of importance for a long time. Roll motion being highly nonlinear due to the dependence on the viscous flow becomes difficult for prediction. The potential flow-based methods and solvers fail to explain the behaviour of ships in roll. Various approaches and methods have been used by naval architects and ocean engineers to predict and control roll motion of ships and ship-like floating vessels. The most popular method used for the prediction of roll motion and roll damping is through semi-empirical formulae, based on model tests and simplified theory related to flow dynamics around the hull and appendages of the ships [1–3]. The important outcome of this approach was the component-type roll damping where the total damping is divided into various components [4–6]. This approach experiences a setback due to various reasons, important one being drastic change in roll damping with slightest change in the ship design [7]. The hull shape or design and the location and orientation of the appendages like rudder, skeg, bilge keels and fins affect the flow dynamics around the hull significantly causing variations in the roll damping. The flow dynamics obviously changes with the ship moving at a forward speed and when subjected to waves. A few early attempts to measure and simulate the flow around hulls and sharp appendages like bilge keel and predict roll motion and damping can be found in [8–13]. Recently, a lot of work has been done in this field with the use of URANS simulations and the model experiments for validation purpose. Free and forced roll oscillation studies of ship models are presented in [14–18]. URANS-based simulations at design stage are proving to be a good option in understanding roll motion of ships since roll motion has a strong dependence on viscosity effects of the flow around the hull.

There are experimental and numerical studies which account for the effect of forward speed on roll damping as reported in [17, 19, 20]. The roll damping of ship changes with the change in forward speed. The overall roll damping improves with the increase in forward speed since the hull lift component contributes to damping [4, 20]. This paper presents the experimental and numerical study of free roll decay of a 1:100 scale container ship model. The experiments were carried out in calm water without forward speed for an initial heel angle of 19°. The measured data was then used to validate the URANS simulation of the free roll decay for same initial heel

and zero forward speed. Thereafter, the free roll decay simulations were carried out for two forward speeds of 0.734 m/s (7.34 m/s or 14 knots at full scale) and 1.276 m/s (12.76 m/s or 25 knots at full scale) corresponding to Froude number (Fr) of 0.138 and 0.24 using the length between perpendiculars as reference. The validation of the URANS simulations and the simulation-based study on the effect of forward speed on roll damping are discussed.

2 Experimental Investigation

This section describes the facility, container ship model details and instruments used to carry out the free roll decay experiments in calm water.

2.1 Facility

The experiments of free roll decay of the container ship model were carried out in calm water condition in 4 m flume at the Department of Ocean Engineering, IIT Madras. The flume is 4 m wide, 90 m long and has a water depth of 2.5 m. It is capable of producing regular and irregular water waves with a flap type, hydraulic wave-maker. The opposite end has a beach made of rubble stones which minimises the wave reflection. Since no wave was used for free roll decay experiments, the model was placed midway between the wave-maker and beach. The model was subjected to initial heel of 19° and released to oscillate freely, and the roll motion was measured.

2.2 Container Ship Model

The container ship model has a length overall (L) of 3.01 m and length between perpendiculars (L_p) of 2.88 m. The beam (B) of the model is 0.345 m and a depth (D) of 0.24 m at the midship. The mass properties of the light hull were measured in laboratory using hanging experiments. The model was ballasted to a draft, d of 0.12 m using weights maintaining the roll radius of gyration, K_{xx} to be 36% of beam and pitch radius of gyration, K_{yy} to be 21% of length between perpendiculars. The vertical centre of gravity was calculated using hanging experiments of the light hull and position of the ballast weights. It was also confirmed with the help of inclining experiment in calm water. The hydrostatics from the CAD model was calculated and compared with the measurements as shown in Table 1. The centre of gravity and moment of inertia are reported in Table 2. Figure 1 shows the body plan of the container ship. Figure 2a shows the photographic view of the hanging experiment of

Table 1 Hydrostatics and ship parameters from measurements and CAD

Particulars	Model (1:100)			Prototype
	Measured	CAD	Error %	
Length overall (L)	3.01 m	3.01 m	–	301 m
Length between perpendiculars (L_p)	2.88 m	2.88 m	–	288 m
Beam (B)	0.345 m	0.343 m	0.6%	34.5 m
Draft (d)	0.12 m	0.12 m	–	12 m
Depth (D)	0.24 m	0.24 m	–	24 m
L_p/B	8.397	8.397	–	8.397
L/B	8.725	8.725	–	8.725
Displacement, W	61.983 kg	62.951 kg	1.56%	61.983 tons
LCB (from forward perpendicular)	–	1.438 m	–	143.8 m
VCB (BG)	–	0.069 m	–	6.9 m
LCF (from forward perpendicular)	–	1.585 m	–	158.5 m
TCF	–	0 m	–	0 m
Block coefficient, C_B	–	0.531	–	0.531
Prismatic coefficient, C_P	–	0.599	–	0.599
BM_T	–	0.094 m	–	9.4 m
BM_L	–	5.388 m	–	538.8 m

Table 2 Mass properties of container ship model

Draft, d (m)	Displacement, W (kg)	KG (m)	GM (m)	I_{xx} (kg-m^2)	K_{xx}/B	I_{yy} (kg-m^2)	K_{yy}/L_p
0.12	61.983	0.139	0.024	0.9806	0.3646	22.02	0.207

the ship, and Fig. 2b shows the CAD model of the ship which was used in the CFD simulations.

2.3 Instrumentation

The measurements were recorded in a CPU via a data acquisition instrument, *Spider8*. A dual-axis inclinometer was used to measure angular displacements of the

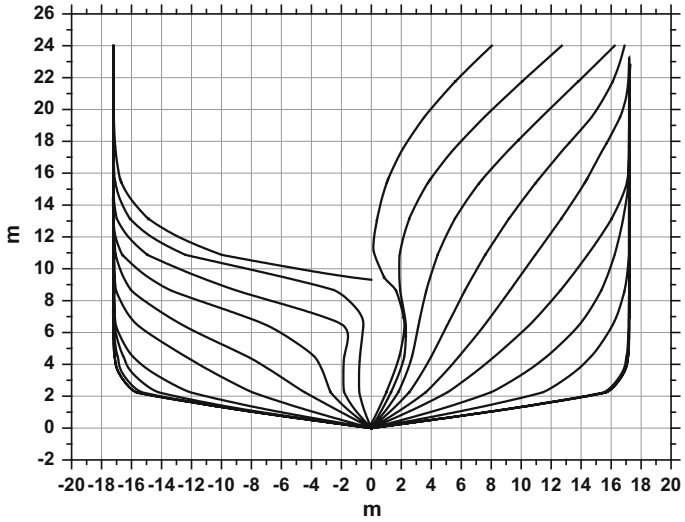

Fig. 1 Body plan of the container ship (full scale)

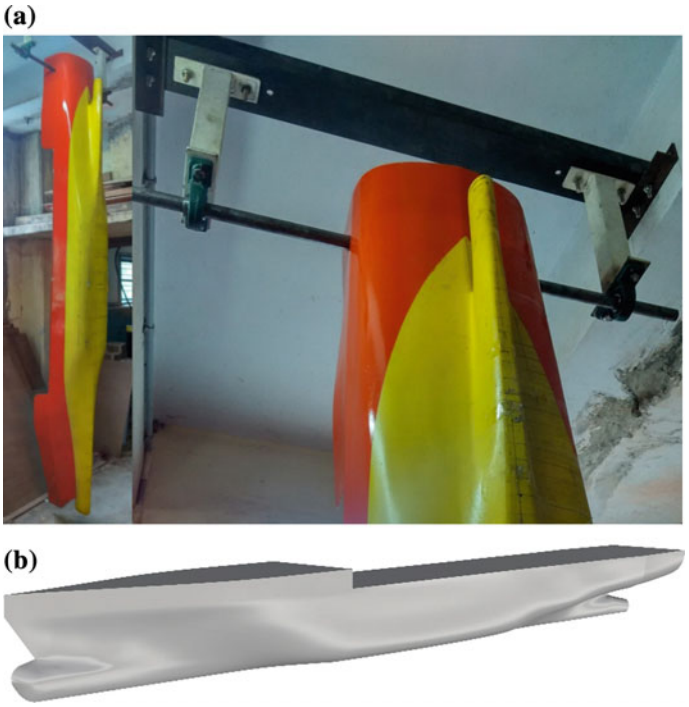

Fig. 2 **a** Photographic view of hanging experiment **b** CAD model of the container ship

container ship. The microelectromechanical system (MEMS)-based inclinometers have a sensor cell embedded in it. The sensor has a pair of electrodes: one is fixed and the other is free to move on springs. The relative motion of the moving electrode under gravity and the fixed electrode changes the capacitance between them. This change in capacitance is sensed by the sensor and converted into angular displacement. The inclinometer was calibrated in laboratory by inclining it to known angles using a simple tilt stand set-up and recording the voltage output from it. The calibration constant was found to be 25.2 mV/deg. It has a range of ±80° with a resolution of 0.01°.

A resistive wave probe was used for measuring the elevation of the waves radiated from the model. The wave probe is 50 cm long and has two stainless steel rods which act as electrodes. The resistance of the wave probe changes with the depth of immersion of the probe which is reflected as change in voltage output. The wave probe was calibrated by immersing it in calm water through specified depth intervals and recording the corresponding output voltage. The voltage output so obtained was converted into wave elevation through the calibration constant. A wavemeter was used to amplify the signals from the wave probe before sending it to data acquisition system.

2.4 Free Roll Decay

The held-over free roll decay experiments were carried out by holding the model at a known initial heel of 19° and releasing it. The model was free to move in all degrees of freedom, and particular care was taken to minimise the coupling effect between the motions. The experiments were carried out in calm water and zero forward speed. The photographic view of the model installed in 4 m flume is shown in Fig. 3. The experiments were repeated to check the reproducibility of the measurements. The typical roll decay motion of the container ship model is shown in Fig. 4.

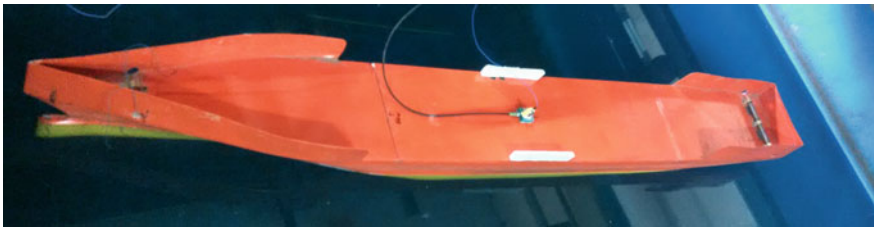

Fig. 3 Container ship model installed in 4 m flume

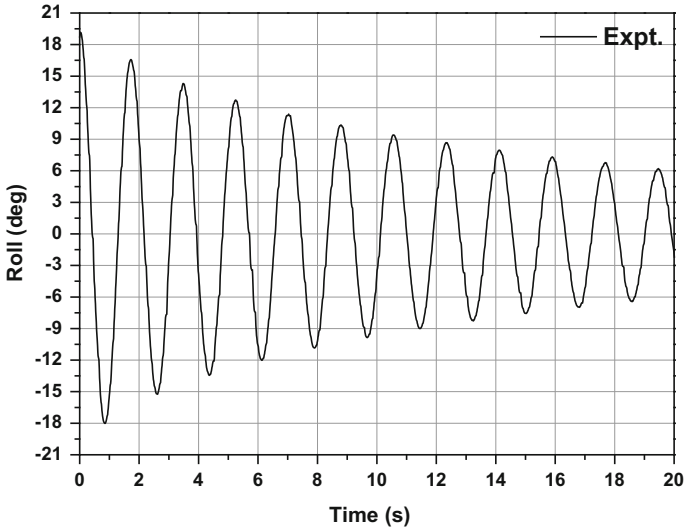

Fig. 4 Roll decay of the container ship ($\varphi_0 = 19°$)

3 URANS Simulations

This section describes the computational domain, meshing and the solver details used to carry out the free roll decay simulations in calm water at zero speed and at two forward speeds as discussed earlier. The three-dimensional (3D) unsteady Reynolds-averaged Navier–Stokes (URANS) simulations of the six-degree of freedom, free roll decay were solved in a commercial software, STAR-CCM+ [21]. The averaged governing equations of continuity and momentum in tensor form for incompressible flow are given in Eqs. (1) and (2), respectively [22].

$$\frac{\partial(\rho\bar{u}_i)}{\partial x_i} = 0; \tag{1}$$

$$\frac{\partial(\rho\bar{u}_i)}{\partial t} + \frac{\partial}{\partial x_j}(\rho\bar{u}_i\bar{u}_j + \rho\overline{u_i'u_j'}) = -\frac{\partial\bar{p}}{\partial x_i} + \frac{\partial\bar{\tau}_{ij}}{\partial x_j} \tag{2}$$

where $\rho\overline{u_i'u_j'}$ is the term representing Reynolds stresses, and $\bar{\tau}_{ij}$ is mean viscous stress tensor. The simulations were solved using segregated flow solver with semi-implicit method for pressure linked equation (SIMPLE) technique for pressure and velocity coupling. Volume of fluid (VOF) method was used for multiphase flow with free surface between air and water as fluids. Implicit unsteady time-stepping with second-order upwind temporal discretization and a second-order upwind scheme for convection was used. A variable time-step scheme based on the Courant number (CFL number) was used with a minimum time-step size of 1e−6. The mean CFL number of 0.5 and target maximum CFL number of 1 were used in the simula-

tion. The convergence limit of 1e−4 and below was achieved for all the continuity, momentum and turbulence variables with ten iterations per time step. The k-ω SST model was used for turbulence modelling in all the simulations since it is suitable for separated flows from near wall. The linear discretized equations were solved using Gauss–Seidel iterative method in the algebraic multigrid (AMG) solver. The initial fluid depth was defined in the flat-wave properties of the VOF wave model, which is used to simulate surface gravity waves. The flat-wave model represents initial calm water condition which can be initialized with current and wind velocities. The coupled motion of the ship model under fluid forces and moments was simulated using dynamic fluid body interaction (DFBI) model allowing free motion in six degrees.

3.1 Computational Domain and Boundary Conditions

The computational domain has similar dimensions as recommended by the ITTC [23]. It extends one L_p on all four sides from the keel, deck, starboard and port at midship of the container as seen in front view of Fig. 5a. The domain extends up to one L_p ahead of forward perpendicular (FP) and up to $2L_p$ behind aft perpendicular (AP) along the ship length as seen in side view in Fig. 5a. The whole domain was divided into two parts: inner moving region or overset region and outer stationary region. The dimensions of the overset regions are also shown in Fig. 5a. It is $3B$ wide, $3D$ deep and $1.5L_p$ long. Figure 5b shows the boundary conditions set for the simulations. All the five sides of the cuboidal stationary domain are set as velocity inlet, and the boundary behind the container ship model is set as pressure outlet. The velocity of water or current can be specified as a vector in Cartesian coordinate system. For a free decay simulation with zero forward speed, the velocity components are set to zero and for simulations with forward speed the X-velocity of the current, i.e. velocity along the ship length is input with a finite value. The two regions are linked with an overset mesh boundary as shown in Fig. 5b. The ship model boundary was set as wall with no-slip. Overset meshes also known as overlapping or chimera mesh are used for a dynamic fluid body interaction (DFBI) simulations and have advantages over remeshing or deforming mesh techniques for high amplitude motions. The inner overset/moving region was given an initial heel along the X-axis at centre of gravity of the ship model before the simulation was started. Linear interpolation scheme was adopted for the connection between the overset and stationary regions which is more accurate but time-consuming.

3.2 Meshing

The meshing was carried out using the software's inbuilt meshing models. Three meshing models were chosen, viz. surface remesher, trimmer and prism layers. Surface remesher is used to retriangulate the existing surface to optimise it for the volume

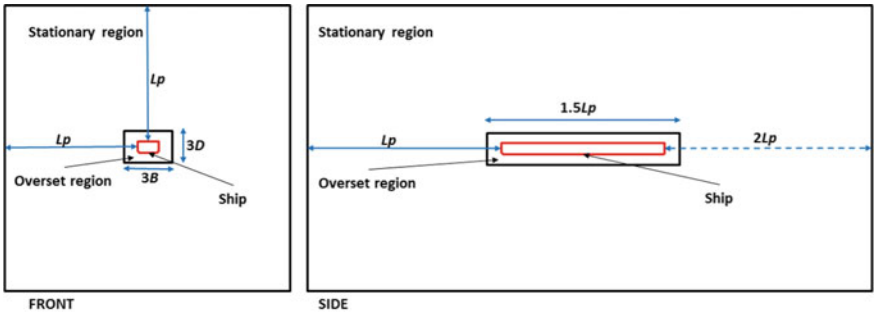

(a) Domain dimensions

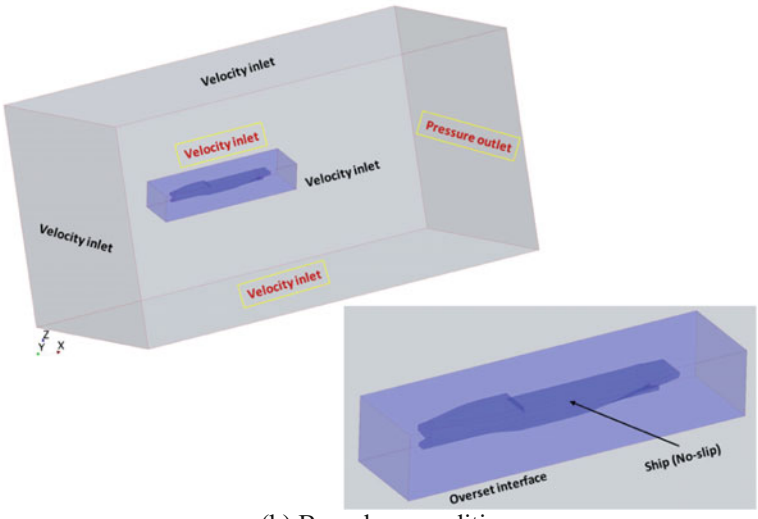

(b) Boundary conditions

Fig. 5 Computational domain

mesh being generated. It can be also used to alter the mesh size on a particular surface. The trimmer meshing model creates predominantly hexahedral cells in the domain, and it trims or cuts off the hexahedral cell according to the surface of the boundary in contact. The resulting mesh is hybrid composed of the structured hexahedral cells and polyhedral cells near the boundaries. The mesh was locally refined near free surface and bilge of the model using separate mesh blocks and surface remesher sizes. Prism layer mesher generates orthogonal prismatic cells near the boundaries used especially for walls with no-slip. It helps to simulate the near wall flow accurately and resolve the boundary layer and separated flow near the walls. The thickness of the prism layer and the number of cells is decided according to the wall $y+$ desired in the flow simulation. In the present simulations, the average wall $y+$ was maintained

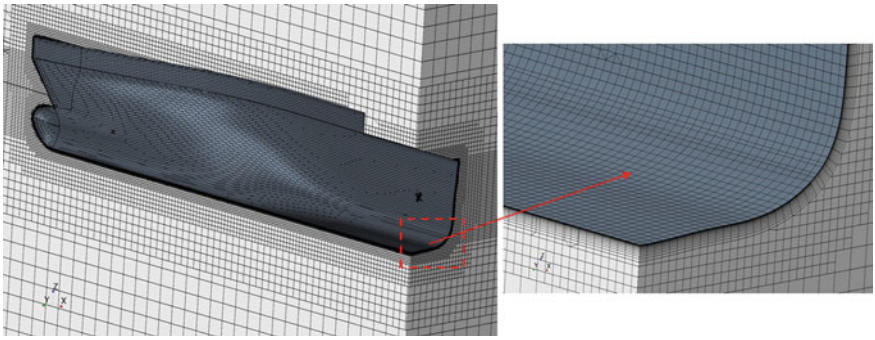

Fig. 6 Computational mesh (fine mesh near free surface and near hull)

below 5 with the *All y+* wall treatment (i.e. wall functions used for low as well as high wall *y+* values), which is a good limit to resolve the near wall flow and separation.

Figure 6 shows the mesh at cut plane along *X*-*Z* and *Y*-*Z* plane for container ship model. The refinement of mesh can be seen near the ship model and free surface. The total cell count for the present simulations is around 2.96 million comprising of stationary region (0.54 million cells) and overset region (2.42 million cells).

4 Results and Discussions

The results from the experimental measurements and URANS simulations are discussed in this section. Initially, the simulation set-up was validated and compared with the experiments for roll decay at zero forward speed, i.e. $Fr = 0$. The simulation set-up was then used to simulate free roll decay at forward speeds of 0.734 and 1.276 m/s corresponding to Fr of 0.138 and 0.24, respectively. Froude number, Fr, is defined in Eq. (3), where V is the ship forward speed or the current speed in case of simulations and g is gravitational acceleration.

$$Fr = \frac{V}{\sqrt{gL_{\mathrm{p}}}} \tag{3}$$

4.1 Validation of URANS with Experiments

The comparison of measured and simulated roll decay is shown in Fig. 7a for $\varphi_0 = 19°$ and $Fr = 0$, i.e. in calm water with zero speed. The URANS simulations were carried out for a physical time of 20 s which covers at least ten roll cycles. The simulated roll motion replicates the experimental measurement closely up to seven cycles, and thereafter, there is slight decrease in motion as compared to experiment. Figure 7b

shows the comparison of measured and simulated damping ratio, ζ plotted versus mean decay angle, φ_m ($(\varphi_n+\varphi_{n+1})/2$) obtained using logarithmic decrement method. Table 3 shows the values of experimental and simulated roll natural period, T_n; ζ and roll added mass, A averaged from first five φ_m. The first half cycle of the decay motion was omitted in the calculation of values in Table 3. The roll natural period compares well with a difference of 0.453% and damping ratio with a difference of 4.762% with experiments taken as reference. It can be seen the comparison between experiments and simulations is reasonably good validating the simulation set-up; to be used for further investigation of the effect of forward speed on roll damping.

4.2 *Effect of Forward Speed on Roll Damping Using URANS*

The simulations of free roll decay with forward speed were carried out by giving the water current velocity in X-direction along the ship length. The ship model was constrained in surge, sway and yaw motions allowing pitch, roll and heave in the simulations with forward speed. The domain was initialised with the constant water current velocity, and the model was given the initial heel of 19° and allowed to roll freely. Figure 8a shows the roll motion obtained from the simulations at $Fr = 0$, 0.138 and 0.24. It can be seen that the ship model subjected to forward speed decays

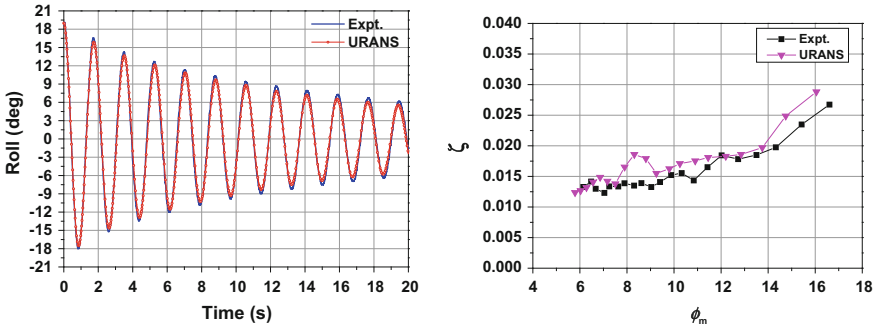

(a) Roll decay

(b) Damping ratio versus mean decay angle

Fig. 7 Comparison from measurement and simulation ($\varphi_0 = 19°$, $Fr = 0$)

Table 3 Validation of natural period, damping ratio and added mass obtained from initial five φ_m

	T_n (s)	ζ	A (kg-m^2)
Expt.	1.760	0.021	0.164
URANS	1.768	0.022	0.175
Difference %	−0.453	−4.762	−6.707

faster as opposed to the zero speed which is in confirmation with the results in [20]. The positive peak roll amplitude at the completion of third cycle is close to 12° for $Fr = 0$, 9° for $Fr = 0.138$ and 5° for $Fr = 0.24$ as can be seen in Fig. 8a. The roll amplitude reduces to below 1.5° after sixth cycle for $Fr = 0.24$, which is indicative of improved roll damping with increasing ship speed. The variation of ζ versus φ_m is shown in Fig. 8b for three Fr. It can be clearly seen that roll damping increases with the increase in forward speed.

Table 4 shows the values of T_n, ζ and A averaged from first five φ_m for three Fr. The roll damping increases by 81.82% for Fr of 0.138 compared with zero forward speed, whereas the damping increases by 65% for $Fr = 0.24$ as compared with $Fr = 0.138$. The roll natural period behaves differently, it increases slightly by 1% for $Fr = 0.138$ as compared with $Fr = 0$, and then, it reduces by 6.89% for $Fr = 0.24$ as compared with $Fr = 0.138$. Similar is the behaviour of roll added mass as shown in Table 4.

Figure 9 shows the roll excitation moments at three Fr. It is observed that the roll excitation moment reduces with increasing forward speed, both at the pressure component (Fig. 9a) and shear component (Fig. 9b). Figure 10 shows the contours of velocity in water at the centre plane along ship length after completion of first roll cycle (see Fig. 8a). In the case of $Fr = 0$, the flow velocities are due to roll motion of the model, whereas in case of $Fr = 0.138$ and 0.24, they are due to both the flow speed and motion of the model. The increased flow velocities for $Fr = 0.138$ and 0.24

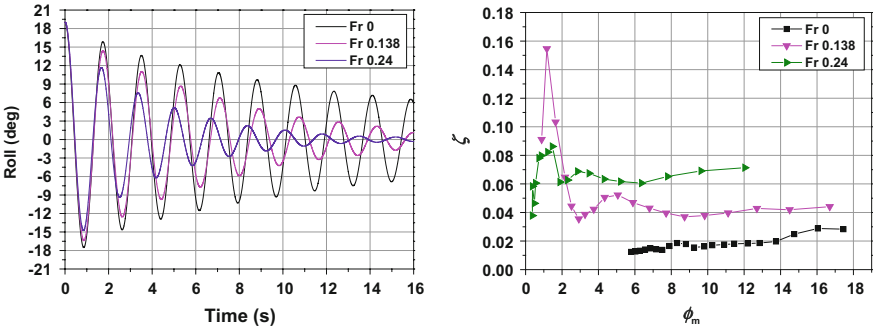

(a) Roll decay

(b) Damping ratio versus mean decay angle

Fig. 8 Simulated free roll decay at three Fr ($\varphi_0 = 19°$)

Table 4 Comparison of natural period, damping ratio and added mass for three Fr

Fr	T_n	ζ	A
0	1.768	0.022	0.175
0.138	1.786	0.040	0.198
0.24	1.663	0.066	0.041

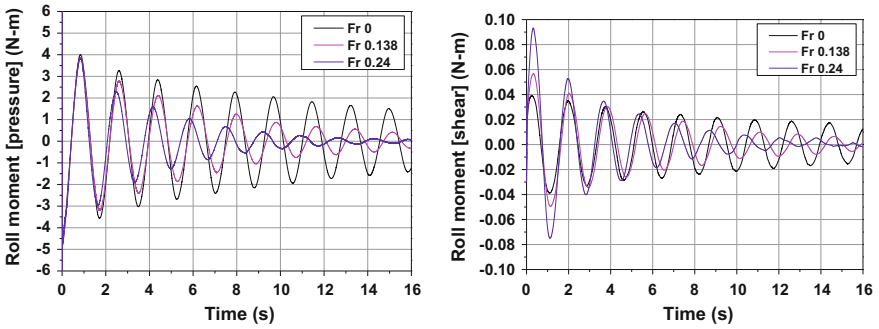

(a) Pressure (b) Shear (skin friction)

Fig. 9 Roll excitation moment at three Fr ($\varphi_0 = 19°$)

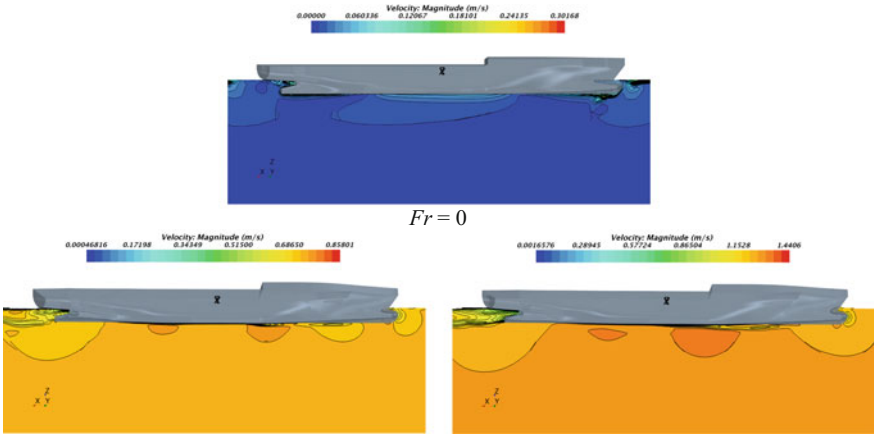

$Fr = 0$

$Fr = 0.138$ $Fr = 0.24$

Fig. 10 Contours of water velocity at three Fr after first roll cycle i.e. $t/T_n = 1$

cause lifting effect on the hull which contributes to both roll damping and restoring moment of the vessel which needs to be studied in detail.

5 Conclusions

Experiments of free roll decay of a container ship were carried out at zero speed, and the measured roll motion was used to validate the URANS-based numerical simulation set-up. The numerical set-up was then used to simulate free roll decay with two forward speeds. It was observed that the roll damping of the container ship increases with forward speed. This was also observed in the past literature, and

the main reason for increase in roll damping is the contribution from hull lift at forward speed. The roll natural period and added mass increase for a forward speed of 0.734 m/s as compared to zero forward speed, whereas roll natural period and added mass decrease for the forward speed of 1.276 m/s as compared to 0.734 m/s and zero forward speed.

Further, investigation on the variation of roll damping and roll natural period needs to be studied by subjecting the ship to various speeds. Experiments can also be conducted in towing tank for free or forced roll oscillation tests at forward speeds.

References

1. Ikeda Y, Himeno Y, Tanaka N (1977) On eddy making component of roll damping force on naked hull. J Soc Nav Archit Jpn 1977(142):54–64
2. Ikeda Y, Komatsu K, Himeno Y, Tanaka N (1977) On roll damping force of ship-effect of hull surface pressure created by Bilge Keels. J Kansai Soc Nav Archit Jpn 165
3. Schmitke RT (1978) Ship sway, roll, and yaw motions in oblique seas. SNAME Trans 86:26–46
4. Ikeda Y, Himeno Y, Tanaka N (1978) Components of roll damping of ship at forward speed. J Soc Nav Archit Jpn 1978(143):113–125
5. Himeno Y (1981) Prediction of ship roll damping-state of art. Michigan, USA
6. Chakrabarti S (2001) Empirical calculation of roll damping for ships and barges. Ocean Eng 28(7):915–932
7. Kawahara Y, Maekawa K, Ikeda Y (2012) A simple prediction formula of roll damping of conventional cargo ship on the basis of Ikeda's method and limitations. J Shipp Ocean Eng 2:201–210
8. Downie MJ, Bearman PW, Graham JMR (1988) Effect of vortex shedding on the coupled roll response of bodies in waves. J Fluid Mech 189:243–264
9. Lian W (1988) A numerical study of two-dimensional separated flow past bluff bodies at moderate KC-numbers. Appl Ocean Res 10(3):114–119
10. Faltinsen OM, Sortland B (1987) Slow drift eddy making damping of a ship. Appl Ocean Res 9(1):37–46
11. Sarpkaya T, O'Keefe JL (1996) Oscillating flow about two and three-dimensional bilge keels. J Offshore Mech Arct Eng 118(1):1
12. Yeung RW, Liao SW, Roddier D (1998) Hydrodynamic coefficients of rolling rectangular cylinders. Int J Offshore Polar Eng 8:241–250
13. Roddier D, Liao S, Yeung RW (2000) Wave-induced motion of floating cylinders fitted with bilge keels. Int J Offshore Polar Eng 10:241–248
14. Yu Y-H, Kinnas SA (2009) Roll response of various hull sectional shapes using a navier-stokes solver. Int J Offshore Polar Eng 19:46–51
15. Chun H, Chun S, Kim S (2001) Roll damping characteristics of a small fishing vessel with a central wing. Ocean Eng 28(12):1601–1619
16. Paterson EG, Wilson RV, Stern F (2003 Nov) General-purpose parallel unsteady RANS ship hydrodynamics code: CFDSHIP-IOWA. IIHR
17. Wilson RV, Carrica PM, Stern F (2006) Unsteady RANS method for ship motions with application to roll for a surface combatant. Comput Fluids 35(5):501–524
18. Irkal MAR, Nallayarasu S, Bhattacharyya SK (2016) CFD approach to roll damping of ship with bilge keel with experimental validation. Appl Ocean Res. 55:1–17
19. Taylan M (2004) Effect of forward speed on ship rolling and stability. Math Comput Appl 9(2):133–145
20. Irvine M Jr, Longo J, Stern F (2013) Forward speed calm water roll decay for surface combatant 5415: global and local flow measurements. J Ship Res 57(4):202–219

21. CD-adapco (2016) STAR-CCM+® Documentation
22. Ferziger JH, Peric M (2002) Computational methods for fluid dynamics. Springer, Berlin
23. ITTC (2011) ITTC-recommended procedures and guidelines: practical guidelines for ship CFD applications. Rio de Janeiro